Chemistry–A European Journal
Research Article
doi.org/10.1002/chem.202303585
Chemistry Europe
European Chemical Societies Publishing
www.chemeurj.org

Ferrocenyl Dinuclear Gold(I) Complexes. Study of their Structural Features and the Influence of Bridging and Phosphane Ligands in a Catalytic Cyclization Reaction

Juan Carlos Pérez-Sánchez,[a, b] Raquel P. Herrera,*[b] and M. Concepción Gimeno*[a]

The combination of the ferrocene moiety with gold(I) catalysis remains a relatively unexplored field. In this article, we delve into the synthesis, characterization, and potential catalytic activity of four complexes utilizing both monodentate and bidentate ferrocenyl diphenylphosphane ligands (ppf and dppf), coordinated with two gold(I) metal centers, linked by either chloride or pentafluorophenylthiolate bridging ligands. This leads to the formation of cationic "self-activated" precatalysts capable of initiating the catalytic cycle without the need for external additives. The catalytic activity of these complexes was assessed through a model reaction in gold(I) catalysis, specifically the cyclization of a *N*-propargylbenzamide to produce an oxazole. In addition, we studied and compared the influence exerted by both the phosphane and the bridging ligand on the performance of these catalysts.

Introduction

Catalysis has emerged as an indispensable tool in contemporary organic synthesis, offering efficient and sustainable methods for constructing complex molecular architectures.[1] Among the plethora of catalytic systems, gold(I) complexes have garnered substantial attention owing to their unique reactivity and remarkable selectivity in diverse transformations.[2,3] The use of different ligands to fine-tune the properties of these gold(I) complexes has further expanded their synthetic utility, offering a platform for tailoring their catalytic activity to suit specific reaction pathways.[4]

One class of ligands that has attracted significant interest in gold catalysis is phosphane scaffolds.[5] However, ferrocenylphosphanes have received relatively little attention. The unique structural features of ferrocene (Fc), with its aromatic sandwich structure and versatile substitution patterns, provide a rich source for designing ferrocenyl phosphane ligands with tailored electronic and steric properties (Figure 1).[6]

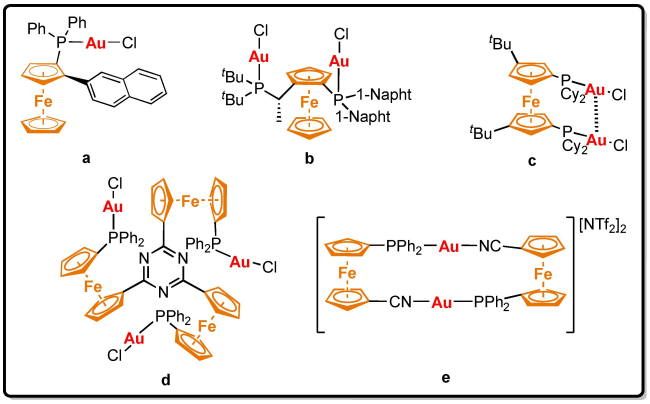

Figure 1. Some selected examples of ferrocenyl phosphane gold(I) complexes employed as catalysts.[7]

Both ferrocenyl mono- and diphosphanes have been extensively explored for their impact on the catalytic behavior of various transition metal complexes of groups 6–10,[8] with a particular emphasis on palladium compounds.[8a] However, there have been significantly fewer studies exploring the combination of the ferrocene scaffold with gold(I) species. Incorporating a ferrocenyl group into phosphane ligands introduces a tunable redox-active unit, which can influence the reactivity of the gold center through electron transfer processes. Additionally, the ability to control the steric environment around the metal center allows for precise control over regio- and stereoselectivity in catalytic transformations.[9]

Typically, in gold catalysis the active species is generated *in situ* through chloride abstraction from [LAuCl] complexes by adding a silver salt containing a weakly coordinating anion, such as $AgSbF_6$ or $AgPF_6$. However, this procedure has two disadvantages: i) the use of an additional metal is required, ii) the utilization of a Ag(I) salt often has a detrimental impact on the reaction outcome due to the non-innocent catalytic behavior of Ag additives ("silver effect").[10] For these reasons,

[a] J. C. Pérez-Sánchez, Prof. Dr. M. Concepción Gimeno
Department of Inorganic Chemistry
Instituto de Síntesis Química y Catálisis Homogénea (ISQCH)
CSIC-Universidad de Zaragoza
C/ Pedro Cerbuna 12, 50009 Zaragoza, Spain
E-mail: gimeno@unizar.es

[b] J. C. Pérez-Sánchez, Prof. Dr. R. P. Herrera
Department of Organic Chemistry
Instituto de Síntesis Química y Catálisis Homogénea (ISQCH)
CSIC-Universidad de Zaragoza
C/ Pedro Cerbuna 12, 50009 Zaragoza, Spain
E-mail: raquelph@unizar.es

Supporting information for this article is available on the WWW under https://doi.org/10.1002/chem.202303585

the utilization of alternative chloride abstractors, along with the design of novel gold(I) catalytic systems, holds special interest in current research.

In recent years, dinuclear gold(I) complexes have emerged as a fascinating class of catalysts in gold catalysis. These species feature two gold centers, typically bridged by a ligand, enabling cooperative effects, and enhancing the catalytic efficiency. The presence of two metal centers provides opportunities for distinct activation pathways, leading to unique reactivity and selectivity profiles not achievable with mononuclear gold(I) catalysts.[11] Notably, Nataro and coworkers have demonstrated the effectiveness of using 1,1′-bis(phosphane)-ferrocene ligands in a wide variety of gold(I) catalyzed reactions.[12]

In this scenario, anion-bridging dinuclear Au^{I} complexes, where the anion can be, for instance, a chloride (also known as chloronium digold complexes)[13] or a thiolate bridge,[14] can act as a source of "naked gold" LAu^{+} species, where L is an ancillary ligand. These dinuclear compounds are self-activated catalysts as they do not need the addition of any additive. Moreover, depending on the bridging anionic ligand, the pivotal LAu^{+} species are originated at different rates to perform the catalytic reaction.

Considering all the comments, here, we present the synthesis, characterization, and structural features of four dinuclear gold(I) complexes, each containing a unique combination of ligands. Specifically, the complexes were designed with ferrocenylmonophosphane (ppf = diphenylphosphaneferrocene) or ferrocenyldiphosphane (dppf = 1,1′-bis(diphenyl)phosphaneferrocene) ligands, along with bridging anions, either chloride or pentafluorophenylthiolate. Notably, these structures showcase distinctive crystalline arrangements where both metallic gold centers assume distinct environment involving (a) Cl or SC_6F_5 bridging ligands, (b) short aurophilic interaction (when present), and (c) a diphosphane chelate.

Herein, our principal objective was to conduct a comparative study of the intricate structural features and redox properties inherent in these ferrocenyl dinuclear gold(I) complexes. Through the elucidation of their structural characteristics, our aim was to achieve a more profound understanding of the factors governing the catalytic behavior of these complexes. Therefore, a complementary objective was to systematically evaluate the influence of both bridging and phosphane ligands, thereby assessing the catalytic activity of these complexes in a model reaction, specifically, the cyclization of a *N*-propargylbenzamide.

Results and Discussion

Synthesis and characterization of ferrocenyl gold complexes

The synthesis of these complexes can be categorized into two distinct groups: those derived from ppf and those derived from dppf (Scheme 1).

Firstly, for the synthesis of monoferrocenylphosphane derivatives, complex **1** was prepared using a previously reported procedure (see ESI, Experimental Section). Subsequently, complex **5** was synthesized by reacting complex **1** with 0.5 equivalents of silver triflate for 30 minutes. During this process, one chloride atom is abstracted from the initial complex, leading to the formation of the chloronium complex $[(\mu\text{-Cl})\{Au(ppf\text{-}\kappa P)\}_2]$ (**5**). The resulting complex was obtained as a yellow powder, being air stable in the solid state. However, it was observed that in aerated solutions, the ferrocene moiety undergoes gradual oxidation, eventually decomposing into Au^{0}, (visually evident as a black residue within the NMR tube).

The ^{1}H NMR spectrum of complex **5** shows the expected resonances associated to the cyclopentadienyl rings of ferrocene as broad singlets along with those assigned to the diphenylphosphane protons (Figure S4). The $^{31}P\{^{1}H\}$ NMR spectrum of complex **5** displays a singlet (Figure S5), at 25.6 ppm corresponding to the $FcPPh_2Au$ unit. This signal was shifted approximately 2.8 ppm to lower frequencies compared to that of complex **1** ($\delta_P = 28.5$ ppm) as previously observed when a monuclear neutral gold(I) phosphane complex turns into a dinuclear cationic complex.[15] The ESI-QTOF high resolution mass spectra reveals a molecular cation peak at m/z 1169.0157 (9%) for complex **5**, while the most intense peak at m/z

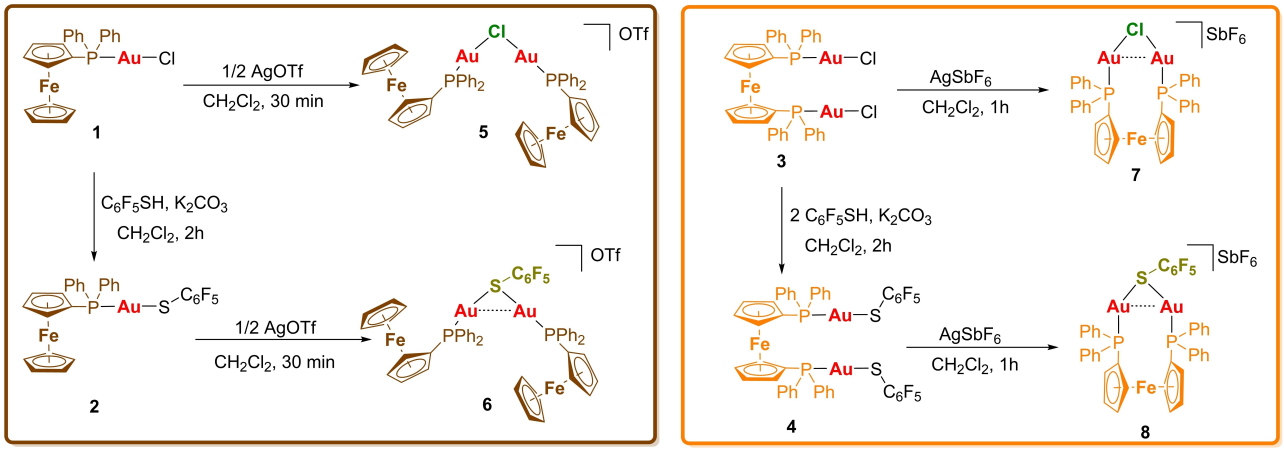

Scheme 1. Synthesis of dinuclear gold(I) complexes derived from ferrocenylphosphanes and chloride or pentafluorophenylthiolate bridging ligands.

937.0842 (100%) observed is in agreement with the $[Au(ppf\text{-}\kappa P)_2]^+$ cation resulting from the loss of a AuCl fragment (Figure S25).

On the other hand, thiolate bridged complex **6** was synthesized from the mononuclear complex **2**. This synthesis involved the reaction of complex **1** with pentafluorophenylthiolate and K_2CO_3. This led to the formation of complex **2**, which was characterized by NMR spectroscopy. The ^{19}F NMR spectrum confirmed the presence of the C_6F_5 ring, displaying three sets of multiplets in a 2:1:2 ratio corresponding to the *ortho*, *para*, and *meta* fluorine atoms, respectively (Figure S3). Additionally, the $^{31}P\{^1H\}$ NMR spectrum (Figure S2) exhibits a unique signal at 32.7 ppm ($\Delta\delta_P = +4.2$ ppm relative to complex **1**).

Similarly, to the procedure used for complex **5**, the reaction of **2** with half an equivalent of AgOTf resulted in the formation of the bridged-type complex **6**. The ^{19}F NMR spectrum, in addition to the resonances associated with the C_6F_5 ring, showed the presence of the triflate anion at −78.0 ppm (Figure S10). Moreover, the ^{31}P NMR spectrum displayed a singlet at 30.3 ppm (Figure S9), again at a lower frequency compared to the mononuclear neutral complex **2**, as previously observed for complex **5**. The ESI-QTOF MS exhibits a similar pattern to that one of complex **5** with molecular cation peak at m/z 1333.0086 (around 9%) and the $[Au(ppf\text{-}\kappa P)_2]^+$ peak at m/z 937.0842 (100%) (Figure S26).

Moreover, complexes **7** and **8** were prepared analogously to the previous complexes, but in this case, using the dppf ligand and the $[Au_2Cl_2(\mu\text{-dppf})]$ (**3**) complex as the starting material. Complex **7** was obtained by reacting **3** with one equivalent of $AgSbF_6$. Along with the precipitation of AgCl, efficient chloride abstraction was confirmed by ^{31}P NMR, which displayed a unique singlet signal at 25.8 ppm (Figure S14), *ca.* 2 ppm upfield shifted compared to $[Au_2Cl_2(\mu\text{-dppf})]$. This trend follows the pattern observed for complexes **5** and **6**. Therefore, while chemical shift values alone may not be sufficient to determine the changes in the geometric environment of the gold(I) atoms, the differences in chemical shift could be associated with a significant reorientation of the phosphorus atoms upon the formation of complexes with bridging ligands. In addition, the mass spectrum of complex **7** exhibits a prominent molecular cation peak at m/z 983.0031 (100%) with no observed fragmentation processes, distinguishing it from complexes **5** and **6** (Figure S27).

Furthermore, complex **8** had been previously described by us,[16] and therefore, it was prepared in a similar manner with slight modifications (see ESI). However, its potential catalytic activity had never been explored before, making it an interesting comparative example with its congener, monophosphane complex **6**. Remarkably, these compounds exhibited higher stability than **5** and **6**, as evidenced by their lack of decomposition over several weeks, both in the solid state and in solution.

The FT-IR spectrum also provides important information regarding the evidence of the formation of bridging ligand complexes. As expected, for both complexes **5** (Figure S7) and **7** (Figure S15), a clear disappearance of the vibration due to $\nu(Au\text{-}Cl)_{terminal}$ is observed. In the parent compounds, this vibration is observed at 333 (vs) cm^{-1} and 336 (vs) cm^{-1} (for complexes **1** and **3**, respectively). However, in the bridged complexes, it is shifted towards lower energies and located at 289 cm^{-1} (complex **5**) or 302 cm^{-1} (complex **7**). The ratio $\nu(Au\text{-}Cl)_{bridge}/\nu(Au\text{-}Cl)_{terminal}$ is 0.87 or 0.90, respectively, values that are in good agreement with literature data reported for gold(I) and gold(III) complexes.[17]

X-Ray diffraction studies

Complexes **2**, **6**, and **7** were successfully crystallized, allowing us to elucidate their molecular structures. It is worth noting that the structure of complex **8** bearing a ClO_4 anion had been previously published by us,[16] which adds a valuable point of reference for our comparisons. Attempts to crystallize complex **5** were futile, as in all cases, the crystallized species turned out to be complex **1**.

Complex **2**, as shown in Figure 2, crystallizes as a single molecule. The metal center in this complex exhibits a slightly non-linear coordination environment, with a P1-Au1-S1 angle of 170.61(2)°. This structural feature is consistent with gold(I) phosphine thiolate complexes.[18]

Turning to complex **6**, the X-ray diffraction analysis, shown in Figure 3, revealed an intriguing structure. The asymmetric unit contains two independent formula units, and an intermolecular Au···Au interaction is evident, with a Au2-Au3 distance of 3.1302(7) Å. Additionally, there are two intramolecular aurophilic interactions in each independent molecule (Au1-Au2 2.9685(6) Å; Au3-Au4 3.0022(6) Å). This structural framework exhibits similarities to those found in complex **8**, which employs the dppf ligand.[16] Notably, these intermolecular aurophilic interactions can be correlated with the bond dissociation energy between the two molecular entities, according to an equation proposed by Schwerdtfeger and coworkers,[19] with values of $D_e = 22.2$ kJ·mol^{-1} and $D_e = 39.3$ kJ·mol^{-1} for com-

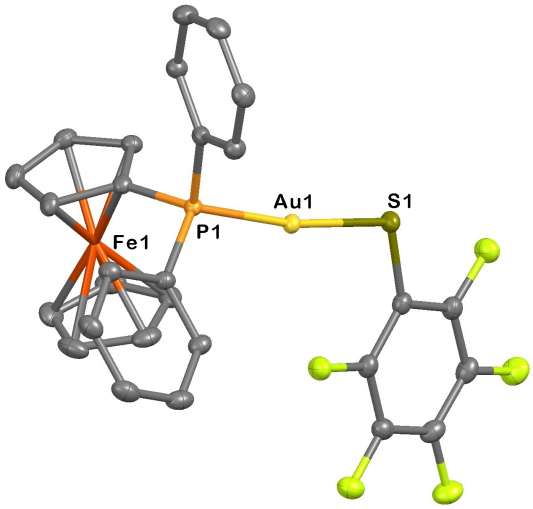

Figure 2. Depiction of the molecular structure of complex **2**. Hydrogen atoms are omitted for clarity. Selected bond lengths [Å] and angles [°]: P1-Au1 2.2534(5), Au1-S1 2.3013(6); P1-Au1-S1 170.61(2).

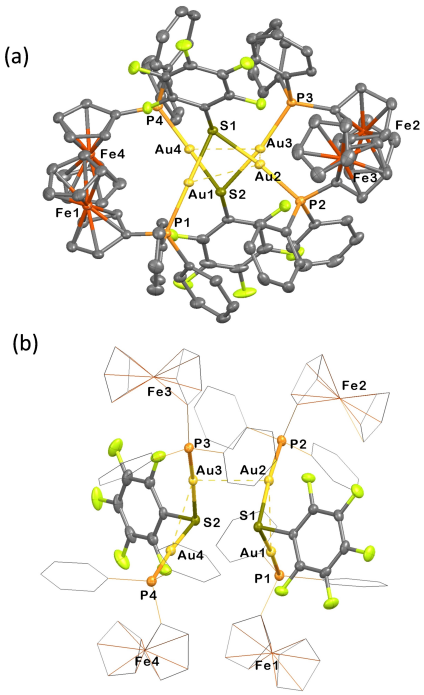

Figure 3. (a) Depiction of the molecular structure of complex **6**·2 CH_2Cl_2, (b) simplified structural diagram of complex **6**·2 CH_2Cl_2. Hydrogen atoms, triflate anions and dichloromethane molecules are omitted for clarity. Selected bond lengths [Å] and angles [°]: P1-Au1 2.2631(7), Au1-Au2 2.9685(6), Au1-S1 2.3551(7), Au2-S1 2.3711(7), Au2-Au3 3.1302(7), Au3-Au4 3.0022(6), Au4-S2 2.3490(7), Au3-S2 2.3627(7), Au1-Au4 4.2566(7); Au1-S1-Au2 77.82(2), Au3-S2-Au4 79.16(2), P1-Au1-S1 175.89(3).

plexes **6** and **8**, respectively. Furthermore, the Au-S-Au angles in **6** are very narrow, 77.82(2)°, and similar to those found in complex **8**, with a value of 77.59(17)°.

The X-ray diffraction structure of complex **7**, showcased in Figure 4, reveals remarkable insights into its structure. One noteworthy observation is the close proximity of the two gold metal centers, resulting in an exceptionally short Au···Au contact of 2.8828(6) Å. This distance is notably shorter than the one observed in complex, $[Au_2(\mu\text{-Cl})(PPh_3)_2][ClO_4]$, showing a Au-Au distance of 3.085(2) Å.[13a] This disparity underscores a strong aurophilic interaction within complex **7**, further facilitated by the flexible ligand dppf that allows the metal centers to approach each other closely. Although the existence of a single chloride bridging ligand between two Au^{I} centers is not exceedingly rare, the Au···Au interaction observed in complex **7**, as far as we are aware, is among the shortest reported for gold(I) chloronium complexes.[13] Moreover, the structural analysis reveals a P1-Au1-Cl1 angle of 173.01(4)°. However, the Au1-Cl1-Au2 angle, is significantly narrow, with a value of 75.27(4)°, compared to the complex $[Au_2(\mu\text{-Cl})(PPh_3)_2]^+$, which features an angle of 82.7(2)°, thus favoring the Au···Au interaction.

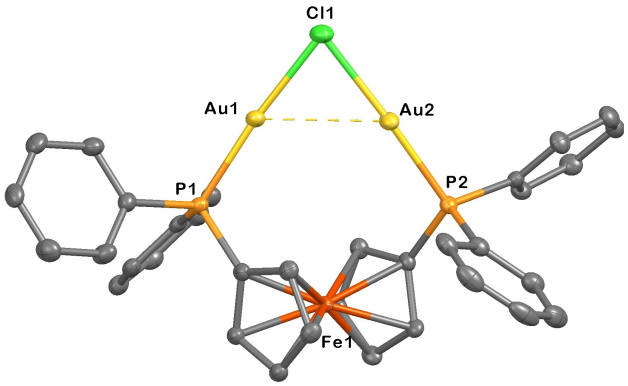

Figure 4. Depiction of the molecular structure of complex **7**·Et_2O. Hydrogen atoms, a Et_2O molecule and SbF_6^- anion are omitted for clarity. Selected bond lengths [Å] and angles [°]: P1-Au1 2.229(1), Au1-Cl1 2.357(1), P2-Au2 2.228(1), Au2-Cl1 2.363(1), Au1-Au2 2.8828(6); P1-Au1-Cl1 173.00(4), Au1-Cl1-Au2 75.28(4).

Electrochemical characterization

The complexes **5**–**8** were studied by cyclic voltammetry in a 0.5 mM solution in dichloromethane over the electrochemical window of −200 to 1800 mV (Figure 5, see ESI for more information).

In all cases, they displayed both single reversible oxidation ($Fe^{II}\rightarrow Fe^{III}$) and reduction waves ($Fe^{III}\rightarrow Fe^{II}$), centered on the ferrocene unit. For the monophosphane complexes **5** and **6**, they exhibited half-wave potentials values of 0.38 V and 0.35 V, respectively, which are slightly higher than that of complex **1** ($E_{1/2}$ = 0.32 V).[20] This could be tentatively attributed to the cationic nature of these complexes. In contrast, dppf derived complexes, **7** and **8**, showed $E_{1/2}$ values around 0.76 V, exhibiting an anodic shift of roughly 40 mV compared to the monophosphane derivatives. This deviation suggests enhanced electron donation from the dppf fragment to Au, as opposed to ppf. Consequently, this leads to a depletion of electron density on the ferrocene unit, thereby difficulting the oxidation process. Importantly, a significant anodic shift is observed in the cationic bridging complexes, as exemplified by complex **7** ($E_{1/2}$ = 0.76 V) relative to complex **3** ($E_{1/2}$ = 0.64 V).[21] This observation under-

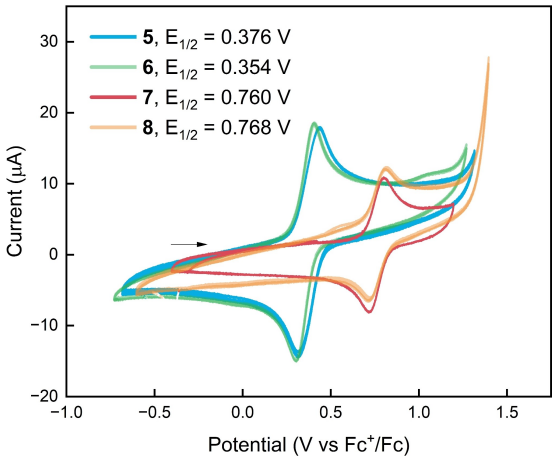

Figure 5. Superimposition of cyclic voltammograms of 0.5 mM solutions of complexes **5** (blue), **6** (green), **7** (red) and **8** (orange) in CH_2Cl_2/0.1 M $[Bu_4N][PF_6]$ at 100 mV/s, in the electrochemical window of −200 mV to 1800 mV, referenced against Fc^+/Fc couple.

scores that the presence of a charge involving the gold(I) centers withdraws electron density from either the ppf or dppf fragment, thereby hindering the oxidation of the ferrocene unit.

Furthermore, it is noteworthy to highlight the values of anodic and cathodic current intensities. Complexes **5** and **6** displayed values approximately twice those of complexes **7** and **8**. This can be attributed to the presence of two Fe centers, one per each ferrocene unit, in contrast to a single Fe center for the diphosphane complexes. This suggests that both ferrocene moieties are oxidized (and reduced) simultaneously in **5** and **6**, in the same step, without a significant electronic coupling between the two units.

In all cases, the voltammograms were fitted to the Randles-Ševčík equation (see ESI), indicating the chemical reversibility of the system. However, deviations from linear fitting were observed for **5** (Figure S28) and **6** (Figure S29) compared to **7** (Figure S30) and **8** (Figure S31). In terms of electrochemical reversibility, which can be inferred from the shape and characteristics of the cyclic voltammograms, it is noteworthy that the separation between the anodic peak potentials ($E_{p,a}$) and cathodic peak potentials ($E_{p,c}$) exceeded the theoretical value predicted by the Nernst equation, which is typically 59/n mV (where n represents the number of electrons involved in the redox process). This deviation suggests the presence of increased solution resistance in the analyzed solutions (see Table S1).

Catalytic study

The previously described dinuclear gold(I) complexes offer a unique opportunity to explore the influence of various factors on their catalytic activity, with a specific focus on the comparison between ferrocenyldiphosphanes and ferrocenylmonophosphane ligands. Additionally, the impact of bridging ligands on these complexes is of special interest, as these types of ligands are often used to facilitate the formation of LAu^+ species as previously discussed. Understanding the role of bridging chloride or thiolate anions in these dinuclear gold(I) complexes could provide valuable insights into their catalytic behavior. Then, in this study we assess the influence exerted by (a) the anionic bridging ligand, considering four complexes, in terms of its lability to generate the catalytically active species $[LAu]^+$, and we explore the impact of (b) the use of monophosphanes versus diphosphanes acting as chelates.

To evaluate the catalytic activity of these complexes, we performed the *5-exo-dig* cyclization of a *N*-propargylbenzamide to an oxazole, which is a well-established benchmark reaction in gold(I) catalysis.[22–24] Specifically, we investigated the cyclization of 4-fluoro-*N*-(prop-2-yn-1-yl)benzamide (**9**) to form 2-(4-fluorophenyl)-5-methylene-4,5-dihydrooxazole (**10**) (Scheme 2). The choice of a *para*-fluoro-substituted ring in the substrate **9**, allows a simplification of the ^{1}H NMR spectrum, making it easier to monitor the reaction progress and facilitates tracking of the cyclization process by ^{19}F NMR monitoring.

The cyclization reaction was carried out using a catalytic loading of 5 mol% in $CDCl_3$ at room temperature (for more

Scheme 2. Gold(I)-catalyzed cyclization of propargyl amide **9** to oxazoline **10**.

experimental details, see the Supporting Information), and the summarized results are presented in Table 1.

The catalytic performance of complexes **5** and **7**, (chloride bridging ligands), was notably high (Table 1, entries 1 and 3). These complexes achieved complete conversions of substrate **9** within a period of 2 hours, with yields of 94% (TOF = 9.4 h^{-1}) and 96% (TOF = 9.6 h^{-1}), respectively.

In contrast, complexes **6** and **8**, (thiolate bridging ligands), displayed distinct catalytic results. While complex **6** exhibited a moderate conversion of 68% after 2 hours (TOF = 6.8 h^{-1}) (Table 1, Entry 2), complex **8** only gave product **10** with 38% yield under identical conditions, with a significantly lower TOF = 3.8 h^{-1} (Table 1, Entry 4).

The complexes described in our study with bridging ligands could be identified as "self-activated" gold(I) catalysts. By exploiting the lability of the bridging ligand, these complexes act as a source of LAu^+ responsible for the cyclization reaction.

Therefore, we have selected the $Ph_3PAuNTf_2$ as a benchmark catalyst for comparison. This selection is not arbitrary; it is grounded in the participation of Ph_3PAu^+ in the gold(I) catalyzed reaction.[25] This parallels the behavior observed in complexes **5** and **6**, where the active species in the catalytic cycle is tentatively assigned to the $FcPPh_2Au^+$ cation. In Table 1, Entry 5, the results with this "self-activated catalyst" (acting as PPh_3Au^+ in solution), were included. Complex $Ph_3PAuNTf_2$ provided a yield of 68% in 3 hours (TOF = 4.5 h^{-1}). Notably, complexes **5** and **7** displayed enhanced catalytic activity, with TOF values more than twice that of $[PPh_3Au(NTf_2)]$.

Table 1. Catalytic results of the *5-exo-dig* cyclization of propargyl amide **9** to oxazoline **10**.

Entry[a]	$[Au]_{cat.}$	Yield[b] (%)	TON[c]	TOF[d] (h^{-1})	$TOF_{initial}$[e] (h^{-1})
1	**5**	94	18.8	9.4	19.4
2	**6**	68	13.6	6.8	18.1
3	**7**	96	19.2	9.6	15.0
4	**8**	38	7.6	3.8	2.3
5[f]	**$[PPh_3AuNTf_2]$**	68	13.6	4.5	n.d.[g]

[a] Reactions conditions: 0.05 mmol of **9**, 0.0025 mmol (5 mol%) catalyst, 0.500 mL of $CDCl_3$, 20–25 °C (rt), 2 h. [b] Determined by ^{1}H NMR using 1,3,5-trimethoxybenzene as internal standard. Percentages correspond to the average of three independent experiments. [c] TON calculated as mmol of product / mmol of catalyst. [d] TOF calculated as TON / time, in a period of 2 h. [e] Initial TOF calculated as the slope of the TON vs time plot, (conversion < 50%), (see ESI). [f] Reference [22a], yield reported after 3 h. [g] Not determined.

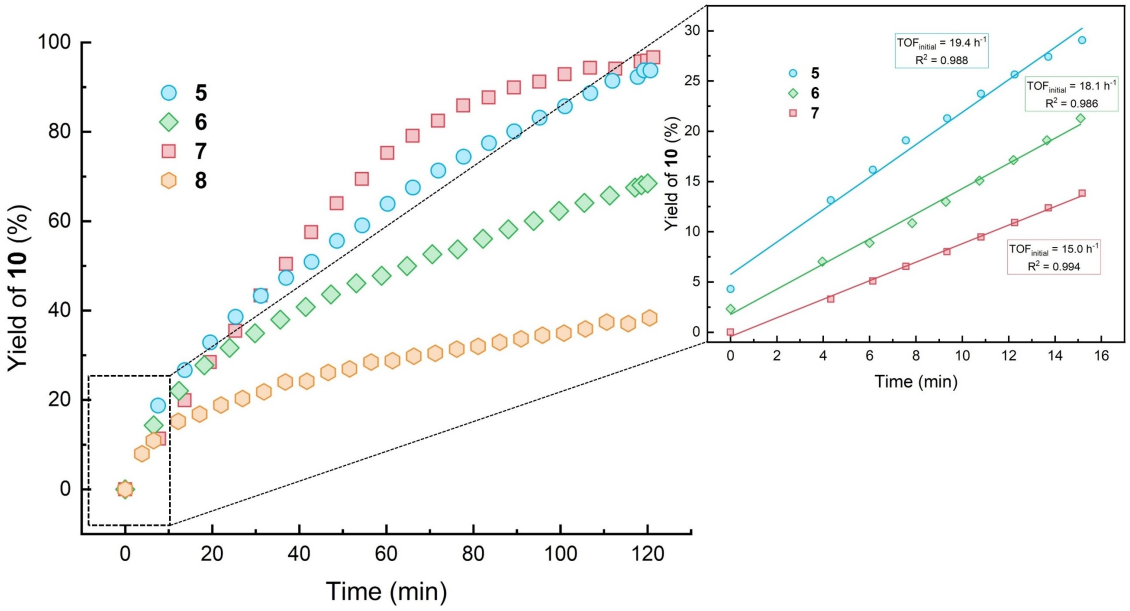

Figure 6. Kinetic profiles of the gold(I) catalyzed (complexes **5**–**8**) cyclization of **9** to **10** and detail of the initial moments of the reaction (15 minutes) for complexes **5**–**7**.

Furthermore, a detailed analysis of the kinetic profiles of the catalysts revealed some differences among the studied complexes (Figure 6).

The complexes bearing chloride bridges demonstrated to catalyze significantly faster the cyclization reaction compared to those with pentafluorophenylthiolate bridges. Notably, complexes **5** and **6**, despite showing similar catalytic activities, displayed distinct kinetic behavior when monitored through ^{1}H NMR during the initial stages (< 20 min) of the reaction (see ESI, Catalytic Studies). The initial TOFs calculated (Figure S33) for **5** (19.4 h^{-1}, Table 1, entry 1) and **6** (18.1 h^{-1}, Table 1, entry 2) were notably higher than the initial TOF of complex **7** (15.0 h^{-1}, Table 1, entry 3), indicating a higher conversion rate during this early period. However, after 60 minutes of reaction, the performance of complexes **5** and **6** decreased, while complex **7** showed an enhanced catalytic activity. Although, the chloride-bridged complexes **5** and **7** initially exhibited different reaction rates (Figure 6), their overall catalytic performance converged as the reaction progressed. In contrast, complexes **6** and **8**, featuring thiolate bridges, consistently demonstrated lower catalytic activity throughout the reaction, underscoring the substantial impact of the bridging ligand on the overall reactivity.

Previous studies have established that the *5-exo-dig* cyclization reaction follows a first-order behavior with respect to the substrate using similar catalytic systems.[24f] Our studies confirmed this first-order kinetics by plotting ln([**9**]/[**9**]$_0$) *vs* time, for all the complexes studied. However, for complex **5**, the linear fit deviates from first-order kinetics at higher conversion values (Figure 7).

Several factors may contribute to this deviation, with one plausible explanation being the reduced stability of catalyst **5**. It is conceivable that the complex **5** undergoes decomposition,

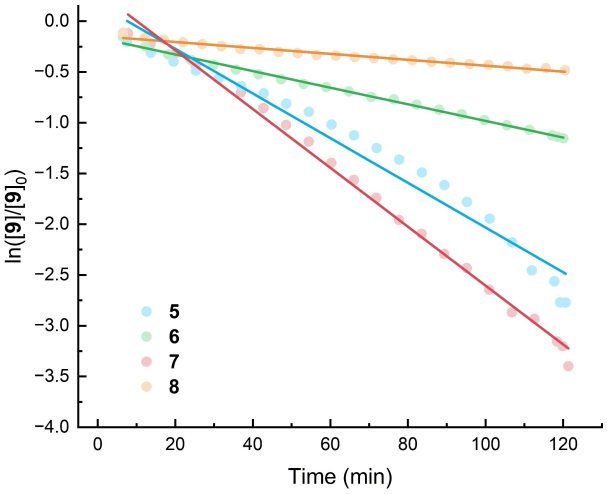

Figure 7. Variation of the ln([**9**]/[**9**]$_0$) profile with the reaction time at room temperature for catalysts **5**–**8**.

leading to the formation of deactivated species, such as L_2Au^+, Au(0), and other unidentified gold species.[26] Indeed, the most abundant species observed in the mass spectrum of complex **7** was $[Au(ppf\text{-}\kappa P)_2]^+$ (Figure S27), supporting the idea of catalyst decomposition and speciation.

To further investigate the catalytic behavior, we calculated the kinetic rate constants within the linear range from 0 to 30 minutes for all the complexes (see ESI, Figure S34). The resulting rate constants exhibited a wide range, spanning from 2 to 18 min^{-1}. As initially hypothesized, catalyst **7** demonstrated to be the most efficient and fastest reacting catalyst among the complexes studied. On the other hand, complex **8** displayed a rate constant nearly eight times lower than its chloride-bridged

analogue, indicating a significant difference in its catalytic activity.

Considering the two factors studied among the complexes, it can be concluded that the nature of the bridging ligand significantly influences the catalytic activity. Complexes containing the diphosphane ligand dppf (complexes **7** and **8**) showed a marked difference in their catalytic performance between the chloride-bridged complex **7** and the thiolate-bridged complex **8**. Similarly, this trend was observed for complexes with the monophosphane ligand ppf (complexes **5** and **6**), with the chloride-bridged complex demonstrating better catalytic activity.

Additionally, when comparing the influence of monophosphane and diphosphane ligands, it is evident that for complexes **5** and **7** (both with chloride bridging ligands), there is no significant difference in their catalytic performance, as they achieved very similar conversions. However, for complexes with thiolate bridges, using a monophosphane ligand (complex **6**), resulted in better yields compared to the diphosphane ligand (complex **8**).

Conclusions

Our examination of the structural features of a series of ferrocenyl dinuclear gold(I) complexes, showcasing diverse combinations of ferrocenylphosphane ligands and bridging ligands, has revealed some intriguing properties. Firstly, the examination of redox activity centered on the ferrocene unit highlighted distinct features between monophosphane and diphosphane complexes. This underscores the critical influence of the phosphane ligand, while surprisingly, the bridging ligand exhibited apparent non-influence on the oxidation and reduction potential of the ferrocene moiety. It is noteworthy, that complexes derived from monophosphane (**5** and **6**) were oxidized at lower potentials, whereas those derived from diphosphane (**7** and **8**) were oxidized at higher potentials than their monophosphane counterparts. This observation could provide some insights into the tailored redox characteristics achievable by just manipulating the phosphane ligand.

In a complementary exploration of their catalytic potential, our study revealed that these structurally diverse dinuclear gold(I) complexes displayed interesting catalytic behaviors. The choice of both phosphane and bridging ligands played a crucial role in influencing catalytic activity. Chloride-bridged complexes **5** and **7** demonstrated remarkable catalytic efficiency, surpassing the performance of the tested benchmark catalyst within a short reaction time. Thiolate-bridged complexes **6** and **8**, on the other hand, exhibited a distinct catalytic landscape with varying conversion rates. Furthermore, kinetic analysis underscored the critical role of the bridging ligand, as catalyst **7** emerged as the fastest reacting among all, while complex **8** exhibited a significantly lower rate constant. Notably, while our primary objective centered on elucidating the structural intricacies of these complexes, the observed catalytic behaviors provided an additional layer of understanding, highlighting the multifaceted nature of these compounds.

Eventually, the nature of the bridging ligand plays a pivotal role in influencing the catalytic activity of these dinuclear gold(I) complexes. The choice of phosphane ligands, whether monophosphane or diphosphane, also introduces noteworthy variations in their performance. These findings contribute to our understanding of catalysts design and offer a valuable avenue for tailoring catalytic systems in future studies.

Experimental section

General procedures and materials: All experiments and manipulations were carried under air unless, otherwise stated (standard Schlenk techniques). ^{1}H, ^{19}F and ^{31}P NMR spectra were recorded on a Bruker Avance 300 or 400 at the indicated frequencies at 298.15 K. Chemical shifts are reported in ppm and referenced to $SiMe_4$, using the internal signal of the deuterated solvent as reference (^{1}H) and external H_3PO_4 85% (^{31}P) or external $CFCl_3$ (^{19}F). Multiplicity of the observed signals is indicated as follows: s = singlet, br s = broad singlet, d = doublet, dd = doublet of doublets, m = multiplet. *J* values are given in Hz. Infrared spectra were recorded (in solid) in the range 4000–250 cm^{-1} on a PerkinElmer Spectrum 100 FTIR spectrometer equipped with an ATR accessory, the type of signal is denoted as follows: s = strong, vs = very strong, m = medium, w = weak. High resolution mass spectra of complexes were acquired on a Bruker MicroTOF-Q (ESI+) spectrometer. Electrochemical experiments were performed by means of an EG&G Research Model 273 potentiostat/galvanostat. A three-electrode glass cell consisting of a glassy carbon disk working electrode, a platinum-wire auxiliary electrode, and a Ag/AgCl (3 M) reference electrode was employed. The supporting electrolyte solution (NBu_4PF_6, 0.1 M) was scanned over the solvent window (CH_2Cl_2) to ensure the absence of electroactive impurity curves. A concentration of complexes **5**–**7** of about 5×10^{-4} M was employed in all the measurements. A total of five cycles were acquired for each respective scan rate. All solvents were degassed and dried prior using over activated 3 or 4 Å molecular sieves. All chemical reagents were purchased from commercial suppliers and used as received. The starting materials [AuCl(tht)],[27] ppf (ppf = diphenylphosphaneferrocene),[28] [AuCl(ppf-κ*P*)] (**1**),[20] [Au_2Cl_2(μ-dppf)] (**3**)[29] (dppf = 1,1′-bis(diphenylphosphane)ferrocene), [$Au_2(SC_6F_5)_2$(μ-dppf)] (**4**)[16] and 4-fluoro-*N*-(prop-2-yn-1-yl)benzamide (**9**)[22a] were prepared according to published procedures. All other reagents were commercially available and were used without further purification.

Crystallography: Crystals suitable for X-ray studies were obtained by vapor diffusion of diethyl ether (**7**) or *n*-hexane (**2** and **6**) over a solution of the corresponding compound in dichloromethane. Crystals were mounted on a MiTeGen Crystal micromount and transferred to the cold gas stream of a Bruker D8 VENTURE diffractometer. Data were collected using monochromated MoKα radiation (λ = 0.71073 Å). Scan type ω. Absorption correction based on multiple scans were applied with the program SADABS.[30] The structures were refined on F^2 using the program OLEX2.[31] All non-hydrogen atoms were refined anisotropically. Hydrogen atoms were included using a riding model. CCDC deposition numbers 2304123 (**2**), 2304124 (**6**) and 2304125 (**7**) contain the supplementary crystallographic data. These data can be obtained free of charge by The Cambridge Crystallography Data Center.

Synthesis of complex [Au(SC_6F_5)(ppf-κ*P*)] (2): To a flame dried Schlenk flask equipped with a stirring bar was added [AuCl(ppf-κ*P*)] **1** (121 mg, 0.2 mmol) and 20 mL of dry and degassed CH_2Cl_2. Then, C_6F_5SH (28 μL, 0.22 mmol) and anhydrous K_2CO_3 (0.6 mmol, 83 mg) were added, and the resulting orange solution was stirred for 2 h.

After this time, the solution was filtered through a short Celite® pad and all the volatiles were removed under reduced pressure. The solid residue was dissolved in CH_2Cl_2 (5 mL) and precipitated by the addition of cold pentane (10 mL). The resulting yellow solid was washed with cold pentane (2×5 mL) and dried under vacuum. Yield (118 mg, 77%). ^{1}H NMR (300 MHz, $CDCl_3$) δ_H (ppm): 7.72–7.36 (m, 10H, PPh_2), 4.57 (br s, 2H, C_5H_4), 4.35 (br s, 2H, C_5H_4), 4.14 (br s, 5H, C_5H_5). ^{31}P{^{1}H} NMR (121 MHz, $CDCl_3$) δ_P (ppm): 32.7 (s, 1 P, PPh_2). ^{19}F NMR (282 MHz, $CDCl_3$) δ_F (ppm): −131.70–−132.6 (m, 2F, *ortho*-C_6F_5), −162.4 (t, $^3J_{F,F}$ = 22.8 Hz, 1F, *para*-C_6F_5), −164.0 (m, 2F, *meta*-C_6F_5).

Synthesis of complex [(μ-Cl){Au(ppf-κ*P*)}$_2$] (5): To a flame dried Schlenk flask equipped with a stirring bar was added [AuCl(ppf-κ*P*)] **1** (121 mg, 0.2 mmol) and 20 mL of dry and degassed CH_2Cl_2. Then, [Ag(OTf)] (26 mg, 0.1 mmol) was added and the resulting orange solution was stirred for 30 min protected from light. After this time, the solution was filtered through a 0.45 μm nylon syringe filter and all the volatiles were removed under reduced pressure. The solid residue was dissolved in CH_2Cl_2 (5 mL) and precipitated by the addition of *n*-hexane (10 mL). The resulting yellow solid was washed with *n*-hexane (2×5 mL) and dried under vacuum. Yield (164 mg, 62%). ^{1}H NMR (300 MHz, $CDCl_3$) δ_H (ppm): 7.66–7.35 (m, 20H, PPh_2), 4.63 (br s, 4H, C_5H_4), 4.41 (br s, 4H, C_5H_4), 4.26 (br s, 10H, C_5H_5). ^{31}P{^{1}H} NMR (121 MHz, $CDCl_3$) δ_P (ppm): 25.6 (s, 1P, PPh_2). ^{19}F NMR (282 MHz, $CDCl_3$) δ_F (ppm): −77.0 (s, 3F, OTf). HRMS (ESI/QTOF) m/z: $[M]^+$ Calcd. for $C_{44}H_{38}Au_2ClFe_2P_2$ 1169.0162; Found 1169.0157. IR ν (cm^{-1}): 1026 m (OTf); 280 vs (Au-Cl_{bridge}).

Synthesis of complex [(μ-SC$_6$F$_5$){Au(ppf-κ*P*)}$_2$] (6): To a flame dried Schlenk flask equipped with a stirring bar was added [Au(SC$_6$F$_5$)(ppf-κ*P*)] **2** (154 mg, 0.2 mmol) and 20 mL of dry and degassed CH_2Cl_2. Then, [Ag(OTf)] (26 mg, 0.1 mmol) was added and the resulting orange solution was stirred for 30 min protected from light. After this time, the solution was filtered through a 0.45 μm nylon syringe filter and all the volatiles were removed under reduced pressure. The solid residue was dissolved in CH_2Cl_2 (5 mL) and precipitated by the addition of *n*-hexane (10 mL). The resulting yellow solid was washed with *n*-hexane (2×5 mL) and dried under vacuum. Yield (208 mg, 70%). ^{1}H NMR (300 MHz, $CDCl_3$) δ_H (ppm): 7.71–7.32 (m, 20H, PPh_2), 4.67 (br s, 4H, C_5H_4), 4.41 (br s, 4H, C_5H_4), 4.24 (br s, 10H, C_5H_5). ^{31}P{^{1}H} NMR (121 MHz, $CDCl_3$) δ_P (ppm): 30.3 (s, 1P, PPh_2). ^{19}F NMR (282 MHz, $CDCl_3$) δ_F (ppm): −78.0 (s, 3F, OTf), −129.5 (br s, 2F, *ortho*-C_6F_5), −154.2 (br s, 1F, *para*-C_6F_5), −160.0 (br s, 2F, *meta*-C_6F_5). HRMS (ESI/QTOF) m/z: $[M]^+$ Calcd. for $C_{50}H_{38}Au_2F_5Fe_2P_2S$ 1333.0114; Found 1333.0086. IR ν (cm^{-1}): 1512 m, 1482 m, 1027 m, 976 m (C_6F_5), 1027 s (OTf).

Synthesis of complex [(μ-Cl)Au$_2$(μ-dppf)] (7): Under air, to a round bottom flask equipped with a stirring bar was added [Au_2Cl_2(μ-dppf)] **3** (204 mg, 0.2 mmol) and 20 mL CH_2Cl_2. Then, [Ag(SbF_6)] (68 mg, 0.2 mmol) was added and the resulting orange solution was stirred for 1 h protected from light. After this time, the solution was filtered through a 0.45 μm nylon syringe filter and all the volatiles were removed under reduced pressure. The solid residue was dissolved in CH_2Cl_2 (5 mL) and precipitated by the addition of diethyl ether (10 mL). The resulting yellow solid was washed with cold diethyl ether (2×5 mL) and dried under vacuum. Yield (215 mg, 88%). ^{1}H NMR (400 MHz, CD_2Cl_2) δ_H (ppm): 7.67–7.53 (m, 20H, PPh_2), 4.63 (br s, 4H, C_5H_4), 4.27 (br s, 4H, C_5H_4). ^{13}C{^{1}H}-APT NMR (101 MHz, CD_2Cl_2) δ_C (ppm): 133.6 (d, $^2J_{C\text{-}P}$ = 14.1 Hz, 8 C, $C_{ortho}PPh_2$), 133.4 (br s, 4 C, $C_{para}PPh_2$), 130.0 (d, $^3J_{C\text{-}P}$ = 12.1 Hz, 8 C, $C_{meta}PPh_2$), 128.3 (d, $^1J_{C\text{-}P}$ = 67.8 Hz, 4 C, $C_{ipso}PPh_2$), 75.2 (s a, 8 C, C_5H_4), 71.4 (d, $^1J_{C\text{-}P}$ = 75.7 Hz, 2 C, $C_{ipso}C_5H_4$). ^{31}P{^{1}H} NMR (162 MHz, CD_2Cl_2) δ_P (ppm): 25.8 (s, 1P, PPh_2). HRMS (ESI/QTOF) m/z: $[M]^+$ Calcd. for $C_{34}H_{28}Au_2ClFeP_2$ 983.0035; Found 983.0046. IR ν (cm^{-1}): 692 m, 653 s (SbF_6).

Synthesis of complex [(μ-SC$_6$F$_5$)Au$_2$(μ-dppf)] (8): Compound **8** was prepared according to a previous published method[16] with some modifications. Under air, to a round bottom flask equipped with a stirring bar was added [Au_2(SC$_6$F$_5$)$_2$(μ-dppf)] **4** (272 mg, 0.2 mmol) and 20 mL CH_2Cl_2. Then, [Ag(SbF_6)] (68 mg, 0.2 mmol) was added and the resulting orange solution was stirred for 1 h protected from light. After this time, the solution was filtered through a 0.45 μm nylon syringe filter and all the volatiles were removed under reduced pressure. The solid residue was dissolved in CH_2Cl_2 (5 mL) and precipitated by the addition of diethyl ether (10 mL). The resulting orange solid was washed with cold diethyl ether (2×5 mL) and dried under vacuum. Yield (210 mg, 80%). The spectroscopic data agree with the values provided in the literature.[16] ^{1}H NMR (400 MHz, $CDCl_3$) δ_H (ppm): 7.59–7.52 (m, 20H, PPh_2), 4.65 (br s, 4H, C_5H_4), 4.25 (br s, 4H, C_5H_4). ^{31}P{^{1}H} NMR (162 MHz, $CDCl_3$) δ_P (ppm): 29.0 (s, 1P, PPh_2). ^{19}F NMR (376 MHz, $CDCl_3$) δ_F (ppm): −129.22 (m, 2F, *ortho*-C_6F_5), −153.19 (br s, 1F, *para*-C_6F_5), −159.36 (br s, 2F, *meta*-SC_6F_5). IR ν (cm^{-1}): 692 m, 655 s (SbF_6), 1514 m, 1488 m, 978 m, 851 m, 747 m (C_6F_5).

Acknowledgements

The authors also thank Agencia Estatal de Investigación (PID2020-117455GB-I00 and PID2022-136861NB/AEI/10.13039/501100011033) and Gobierno de Aragón (Research Group E07_23R) for financial support of our research. J. C. Pérez-Sánchez also thanks the Spanish Ministerio de Universidades for a predoctoral grant (FPU21/01888).

Conflict of Interests

The authors declare no conflict of interest.

Data Availability Statement

The data that support the findings of this study are available in the supplementary material of this article.

Keywords: Ferrocene · Gold · Catalysis · Phosphane · Redox

[1] C. A. Busacca, D. R. Fandrick, J. J. Song, C. H. Senanyake, *Adv. Synth. Catal.* **2011**, *353*, 1825–1864.
[2] R. P. Herrera, M. C. Gimeno, *Chem. Rev.* **2021**, *121*, 8311–8363.
[3] For general gold(I) catalysis selected reviews, see: a) A. S. K. Hashmi, G. J. Hutchings, *Angew. Chem. Int. Ed.* **2006**, *45*, 7896–7936; *Angew. Chem.* **2006**, *118*, 8064–8105; b) M. Rudolph, A. S. K. Hashmi, *Chem. Soc. Rev.* **2012**, *41*, 2448–2462; c) A. S. K. Hashmi, D. F. Toste, (Eds.) *Modern Gold Catalyzed Synthesis*, Wiley-VCH, Weinheim, **2012**, pp 1–389; d) A. S. K. Hashmi, *Acc. Chem. Res.* **2014**, *47*, 864–876; e) M. Joost, A. Amgoune, D. Bourissou, *Angew. Chem. Int. Ed.* **2015**, *54*, 15022–15045; *Angew. Chem.* **2015**, *127*, 15234–15258; f) Y. Wei, M. Shi, *ACS Catal.* **2016**, *6*, 2515–2524; g) D. Campeau, D. F. L. Rayo, A. Mansour, K. Muratov, F. Gagosz, *Chem. Rev.* **2021**, *121*, 8756–8867.
[4] a) W. Wang, G. B. Hammond, B. Xu, *J. Am. Chem. Soc.* **2012**, *134*, 5697–5705; b) D. Malhotra, G. B. Hammond, B. Xu, *Ligand Design in Gold Catalysis and Chemistry of Gold–Oxonium Intermediates; in Homogeneous Gold Catalysis. Topics in Current Chemistry, Vol. 357* (Ed.: L. Slaughter), Springer, Cham, **2014**, pp. 1–23; c) C. Obradors, A. M. Echavarren, *Chem. Commun.* **2014**, *50*, 16–28; d) D. Janssen-Müller, C. Schlepphorst, F. Glorius, *Chem. Soc. Rev.* **2017**, *46*, 4845–4854.

[5] A. Collado, D. J. Nelson, S. P. Nolan, *Chem. Rev.* **2021**, *121*, 8559–8612.
[6] For ferrocenyl phosphane ligands selected reviews, see: a) T. J. Colacot, *Chem. Rev.* **2003**, *103*, 3101–3118; b) R. C. J. Atkinson, V. C. Gibson, N. J. Long, *Chem. Soc. Rev.* **2004**, *33*, 313–328; c) R. G. Arrayás, J. Adrio, J. C. Carretero, *Angew. Chem. Int. Ed.* **2006**, *45*, 7674–7715; d) S. Sankar, M. Bandaru, J. Shah, S. Bhilare, C. Schulzke, A. R. Kapdi, J. Roger, J.-C. Hierso, *Coord. Chem. Rev.* **2023**, *491*, 215250.
[7] a) N. Delpont, I. Escofet, P. Pérez-Galán, D. Spiegl, M. Raducan, C. Bour, R. Sinisi, A. M. Echavarren, *Catal. Sci. Technol.* **2013**, *3*, 3007–3012; b) C. Garcia-Morales, B. Ranieri, I. Escofet, L. Lopez-Suarez, C. Obradors, A. I. Konovalov, A. M. Echavarren, *J. Am. Chem. Soc.* **2017**,*139*, 13628–13631; c) T.-A. Nguyen, J. Roger, H. Nasrallah, V. Rampazzi, S. Fournier, H. Cattey, E. D. S. Carrizo, P. Fleurat-Lessard, C. H. Devillers, N. Pirio, D. Lucas, J.-C. Hierso, *Chem. Asian J.* **2020**, *15*, 2879–2885; d) K. Škoch, I. Císařová, P. Štěpnička, *Chem. Eur. J.* **2015**, *21*, 15998–16004.
[8] a) A. Fihri, P. Meunier, J.-C. Hierso, *Coord. Chem. Rev.* **2007**, *251*, 2017–2055; b) N. Dwadnia, J. Roger, N. Pirio, H. Cattey, J.-C. Hierso, *Coord. Chem. Rev.* **2018**, *355*, 74–100; c) L. Cunningham, A. Benson, P. J. Guiry, *Org. Biomol. Chem.* **2020**, *18*, 9329–9370.
[9] J. C. Pérez-Sánchez, R. P. Herrera, M. C. Gimeno, *Eur. J. Inorg. Chem.* **2022**, *2022*, e202101067.
[10] D. Wang, R. Cai, S. Sharma, J. Jirak, S. K. Thummanapelli, N. G. Akhmedov, H. Zhang, X. Liu, J. L. Petersen, X. Shi, *J. Am. Chem. Soc.* **2012**, *134*, 9012–9019.
[11] a) A. C. A. Bayrakdar, T. Scattolin, X. Ma, S. P. Nolan, *Chem. Soc. Rev.* **2020**, *49*, 7044–7100; b) W. Wang, C.-L. Ji, K. Liu, C.-G. Zhao, W. Li, J. Xie, *Chem. Soc. Rev.* **2021**, *50*, 1874–1912.
[12] a) A. Michaels, O. F. Pritchard, J. S. Dell, M. W. Bezpalko, W. S. Kassel, C. Nataro, *J. Organomet. Chem.* **2019**, *889*, 1–8; b) S. A. Wolfarth, N. E. Miner, N. E. Wasmer, R. K. Gwinn, B. C. Chan, C. Nataro, *J. Organomet. Chem.* **2020**, *906*, 121049; c) N. E. Miner, C. Nataro, *J. Organomet. Chem.* **2022**, *963*, 122283.
[13] a) P. G. Jones, G. M. Sheldrick, R. Uson, A. Laguna, *Acta Crystallogr. Sect. B* **1980**, *36*, 1486–1488; b) W. Micklitz, B. Lippert, G. Müller, P. Mikulcik, J. Riede, *Inorg. Chim. Acta* **1989**, *165*, 57–64; c) V. W. W. Yam, C.-L. Chan, K.-K- Cheung, *J. Chem. Soc. Dalton Trans.* **1996** 4019–4022; d) A. Bayler, A. Schier, H. Schmidbaur, *Inorg. Chem.* **1998**, *37*, 4353–4359; e) P. Schulte, U. Behrens, *Chem. Commun.* **1998**1633–1634; f) M. Contel, A. J. Edwards, J. Garrido, M. B. Hursthouse, M. Laguna, R. Terroba, *J. Organomet. Chem.* **2000**, *607*, 129–136; g) A. Hamel, N. W. Mitzel, H. Schmidbaur, *J. Am. Chem. Soc.* **2001**, *123*, 5106–5107; h) A. Castiñeiras, R. Pedrido, *Dalton Trans.* **2010**, *39*, 3572–3584; i) M. Touil, B. Bechem, A. S. K. Hashmi, B. Engels, M. A. Omary, H. Rabaa, *J. Mol. Struct.* **2010**, *957*, 21–25; j) A. Homs, I. Escofet, A. M. Echavarren, *Org. Lett.* **2013**, *15*, 5782–5785; k) Y. Zhu, C. S. Day, L. Zhang, K. J. Hauser, A. C. Jones, *Chem. Eur. J.* **2013**, *19*, 12264–12271; l) J. Schaefer, A. Kraft, S. Reininger, G. Santiso-Quinones, D. Himmel, N. Trapp, U. Gellrich, B. Breit, I. Krossing, *Chem. Eur. J.* **2013**, *19*, 12468–12485; m) N. Phillips, T. Dodson, R. Tirfoin, J. I. Bates, S. Aldridge, *Chem. Eur. J.* **2014**, *20*, 16721–16731; n) A. Grirrane, E. Álvarez, H. García, A. Corma, *Angew. Chem. Int. Ed.* **2014**, *53*, 7253–7258; *Angew. Chem.* **2014**, *126*, 7381–7386; o) S. A. Bhat, J. T. Mague, M. S. Balakrishna, *Dalton Trans.* **2015**, *44*, 17696–17703; p) M. Wegener, F. Huber, C. Bolli, C. Jane, *Chem. Eur. J.* **2015**, *21*, 1328–1336; q) A. Doddi, D. Bockfeld, A. Nasr, T. Bannenberg, P. G. Jones, M. Tamm, *Chem. Eur. J.* **2015**, *21*, 16178–16189; r) S. F. Hartlaub, N. K. Lauricella, C. N. Ryczek, A. G. Furneaux, J. D. Melton, N. A. Piro, W. S. Kassel, C. Nataro, *Eur. J. Inorg. Chem.* **2017**, *2017*, 424–432.
[14] a) T. J. Robilotto, J. Bacsa, T. G. Gray, J. P. Sadighi, *Angew. Chem. Int. Ed.* **2012**, *51*, 12077–12080; *Angew. Chem.* **2012**, *124*, 12243–12246; b) A. Zhdanko, M. Strçbele, M. E. Maier, *Chem. Eur. J.* **2012**, *18*, 14732–14744; c) R. J. Mudd, P. C. Young, J. A. Jordan-Hore, G. M. Rosair, A.-L. Lee, *J. Org. Chem.* **2012**, *77*, 7633–7639; d) P. C. Young, S. L. J. Green, G. M. Rosair, A.-L. Lee, *Dalton Trans.* **2013**, *42*, 9645–9653; e) R. Visbal, R. P. Herrera, M. C. Gimeno, *Chem. Eur. J.* **2019**, *25*, 15837–15845.
[15] a) J. Schulz, I, Císařová, R. Gyepes, P. Štěpnička, *Angew. Chem. Int. Ed.* **2021**, *60*, 6992–6996; b) L. Demonti, H. Tabikh, N. Saffon-Merceron, N. Nebra, *Eur. J. Inorg. Chem.* **2023**, *26*, e202300042.
[16] O. Crespo, F. Canales, M. C. Gimeno, P. G. Jones, A. Laguna, *Organometallics* **1999**, *18*, 3142–3148.
[17] a) R. Usón, A. Laguna, M. V. Castrillo, *Synth. React. Inorg. Met.-Org. Chem.* **1979**, *9*, 317–324; b) K. Nakamoto, *Infrared Spectra of Inorganic and Coordination Compounds*, Wiley-Interscience, New York, **2014**, p. 285.
[18] S. Watase, T. Kitamura, N. Kanehisa, M. Shizuma, M. Nakamoto, Y. Kai, S. Yanagida, *Chem. Lett.* **2003**, *32*, 1070–1071.
[19] P. Schwerdtfeger, A. E. Bruce, M. R. M. Bruce, *J. Am. Chem. Soc.* **1998**, *120*, 6587–6597.
[20] K. Rössler, T. Rüffer, B. Walfort, R. Packheiser, R. Holze, M. Zharnikov, H. Lang, *J. Organomet. Chem.* **2007**, *692*, 1530–1545.
[21] S. L. Kahn, M. K. Breheney, S. L. Martinak, S. M. Fosbenner, A. R. Kassel, W. S. Dougherty, C. Nataro, *Organometallics* **2009**, *28*, 2119–2126.
[22] For some examples including Au(I)-catalyzed cyclization of substrate **9**, see: a) J. P. Weyrauch, A. S. K. Hashmi, A. Schuster, T. Hengst, S. Schetter, A. Littmann, M. Rudolph, M. Hamzic, J. Visus, F. Rominger, W. Frey, J. W. Bats, *Chem. Eur. J.* **2010**, *16*, 956–963; b) S. Sen, F. P. Gabbaï, *Chem. Commun.* **2017**, *53*, 13356–13358; c) B. Zhou, F. P. Gabbaï, *J. Am. Chem. Soc.* **2021**, *143*, 8625–8630; d) N. V. Tzouras, L. P. Zorba, E. Kaplanai, N. Tsoureas, D. J. Nelson, S. P. Nolan, G. C. Vougioukalakis, *ACS Catal.* **2023**, *13*, 8845–8860.
[23] For some examples of Au(I)-catalyzed *5-exo-dig* cyclization of *N*-propargylbenzamide, see: a) S. Doherty, J. G. Knight, A. S. K. Hashmi, C. H. Smyth, N. A. B. Ward, K. J. Robson, S. Tweedley, R. W. Harrington, W. Clegg, *Organometallics* **2010**, *29*, 4139–4147; b) A. S. K. Hashmi, M. C. B. Jaimes, A. M. Schuster, F. Rominger, *J. Org. Chem.* **2012**, *77*, 6394–6408; c) M. Devillard, E. Nicolas, C. Appelt, J. Backs, S. Mallet-Ladeira, G. Bouhadir, J. C. Slootweg, W. Uhl, D. Bourissou, *Chem. Commun.* **2014**, *50*, 14805–14808; d) L. Biasiolo, A. Del Zotto, D. Zuccaccia, *Organometallics* **2015**, *34*, 1759–1765; e) D. Hueber, M. Hoffmann, P. de Frémont, P. Pale, A. Blanc, *Organometallics* **2015**, *34*, 5065–5072; f) V. H. L. Wong, A. J. P. White, T. S. (A.) Hor, K. K. (M.) Hii, *Adv. Synth. Catal.* **2015**, *357*, 3943–3948; g) Y. Hu, X. Xin, B. Wan, *Tetrahedron Lett.* **2015**, *56*, 32–52; h) O. Seppänen, S. Aikonen, M. Muuronen, C. Alamillo-Ferrer, J. Burés, J. Helaja, *Chem. Commun.* **2020**, *56*, 14697–14700; i) A. Franchino, A. Marti, S. Nejrotti, A. M. Echavarren, *Chem. Eur. J.* **2021**, *27*, 11989–11996; j) N. V. Tzouras, A. Gobbo, N. B. Pozsoni, S. G. Chalkidis, S. Bhandary, K. Van Hecke, G. C. Vougioukalakis, S. P. Nolan, *Chem. Commun.* **2022**, *58*, 8516–8519; k) W.-C. Liu, F. P. Gabbaï, *Chem. Sci.* **2023**, *14*, 277–283.
[24] For selected examples of ferrocenyl Au(I) complexes-catalyzed 5-exo-dig cyclization of *N*-propargylbenzamide, see: a) L. Hettmanczyk, S. Manck, C. Hoyer, S. Hohloch, B. Sarkar, *Chem. Commun.* **2015**, *51*, 10949–10952; b) L. Hettmanczyk, L. Suntrup, S. Klenk, C. Hoyer, B. Sarkar, *Chem. Eur. J.* **2017**, *23*, 576–585; c) S. Klenk, S. Rupf, L. Suntrup, M. van der Meer, B. Sarkar, *Organometallics* **2017**, *36*, 2026–2035; d) S. Vanicek, M. Podewitz, J. Stubbe, D. Schulze, H. Kopacka, K. Wurst, T. Meller, P. Lippmann, S. Haslinger, H. Schottenberger, K. R. Liedl, I. Ott, B. Sarkar, B. Bildstein, *Chem. Eur. J.* **2018**, *24*, 3742–3753; e) P. Veit, C. Volkert, C. Förster, V. Ksenofontov, S. Schlicher, M. Bauer, K. Heinze, *Chem. Commun.* **2019**, *55*, 4615–4618; f) O. Bárta, I. Císařová, J. Schulz, P. Štěpnička, *New J. Chem.* **2019**, *43*, 11258–11262; g) A. Straube, P. Coburger, L. Dütsch, E. Hey-Hawkins, *Chem. Sci.* **2020**, *11*, 10657–10668; h) A. Straube, P. Coburger, M. Michak, M. R. Ringenberg, E. Hey-Hawkins, *Dalton Trans.* **2020**, *49*, 16667–16682.
[25] a) N. Mézailles, L. Ricard, F. Gagosz, *Org. Lett.* **2005**, *7*, 4133–4136; b) I. N. Lykakis, C. Efe, C. Gryparis, M. Stratakis, *Eur. J. Org. Chem.* **2011**, *2011*, 2334–2338.
[26] M. Kumar, M. J. Jasinski, G. B. Hammond, B. Xu, *Chem. Eur. J.* **2014**, *20*, 3113–3119.
[27] R. Usón, A. Laguna, M. Laguna, *Inorg. Synth.* **1989**, *26*, 85–91.
[28] a) A. W. Smalley, *Org. Prep. Proced. Int.* **1978**, *10*, 195–196; b) P. Kübler, J. Sundermeyer, *Dalton Trans.* **2014**, *43*, 3750–3766.
[29] M. C. Gimeno, A. Laguna, C. Sarroca, P. G. Jones, *Inorg. Chem.* **1993**, *32*, 5926–5932.
[30] G. M. Sheldrick, *SADABS*, Program for adsorption correction, University of Göttingen, Göttingen, Germany, **1996**.
[31] a) O. V. Dolomanov, L. J. Bourhis, R. J. Gildea, J. A. K. Howard, H. Puschmann, *J. Appl. Crystallogr.* **2009**, *42*, 339–341; b) L. J. Bourhis, O. V. Dolomanov, R. J. Gildea, J. A. K. Howard, H. Puschmann, *Acta Crystallogr. Sect. A* **2015**, *A71*, 59–71.

Manuscript received: October 29, 2023
Accepted manuscript online: December 5, 2023
Version of record online: January 11, 2024